Geological Survey of Canada

University of Victoria

A Comprehensive Investigation of the Earthquake Magnitude-Frequency Relationship due to Fluid Injection in BC

Ramin M.H. Dokht and Honn Kao

February 20, 2025

Abstract

This study investigates induced seismicity associated with hydraulic fracturing (HF) operations in the South Montney Play of northeastern British Columbia, Canada. We analyze seismic events and HF injection data from January 2017 to August 2023, employing a clustering approach to group HF wells and associated induced seismic events. Our analysis reveals that approximately 83% of induced seismicity clusters are associated with HF operations targeting the Lower-Middle Montney (LMM) formation, despite receiving a lower injected fluid volume compared to the Upper Montney (UM) formation. We calculate b-values and seismogenic indices for individual clusters to assess the potential for induced seismicity. The b-values range from 0.5 to 2.3, while seismogenic indices vary between -2.9 and 0.3. These parameters allow us to estimate magnitude exceedance probabilities for each injection site, providing insights into the likelihood of seismic events exceeding specific magnitudes. Considering both the seismogenic index and b-value is crucial for assessing induced seismicity risk, as they quantify event likelihood and the magnitude distribution of earthquakes. Our findings contribute to a better understanding of the spatial variability of induced seismicity within the South Montney Play and aid in identifying areas with higher risk of induced seismic events.

List of Figures

List of Tables

Introduction

Recent increases in seismicity in Western Canada have been attributed to industrial operations like hydraulic fracturing (HF) targeting unconventional hydrocarbons (Hui et al., 2021, Atkinson et al., 2016). Induced seismicity due to HF operations has emerged as a significant concern, particularly in the South Montney Play in British Columbia, where such activities have resulted in significant seismic events (Babaie Mahani et al., 2019, Peña Castro et al., 2020, Wozniakowska and Eaton, 2020, Jia et al., 2022). Recent studies employing machine learning models have provided critical insights into the spatiotemporal characteristics and controlling factors of HF-induced seismicity in northeastern British Columbia, laying the foundation for seismic hazard assessment and risk mitigation strategies (Wang et al., 2022, 2024).

Several studies have investigated the mechanisms behind injection-induced seismicity in the Montney formation of northeastern British Columbia. The high-pressure injection of fluids into the low-permeability Montney formation leads to elevated pore pressures, reducing the effective normal stress acting on pre-existing faults and promoting fault reactivation and the nucleation of significant induced earthquakes (Yu et al., 2019, Peña Castro et al., 2020, Wozniakowska and Eaton, 2020). The isolated occurrence of mainshocks in the crystalline basement, days after the onset of injection in the shallower Montney formation, indicates rapid fluid pressure increase via high-permeability pathways (Atkinson et al., 2020, Riazi et al., 2020, Verdecchia et al., 2020). Peña Castro et al. (2020) analyzed the 30 November 2018 Mw 4.2 earthquake sequence in the Montney formation, noting that the mainshock may have occurred at approximately 4.5 km depth in the crystalline basement, just two days after injection began at a shallower depth of about 2.5 km, which underscores the direct triggering of seismic events by rapid fluid pressure increases. However, this estimated earthquake depth may not represent the general pattern of seismicity, as most of the aftershocks are reported at shallower

depths. The spatiotemporal scales of induced seismic activity in other regions suggest that fluid diffusion and pressure transfer through high-permeability conduits or fracture networks could play a role in triggering earthquakes at relatively large distances of up to about 10 km from the injection wells, delayed even by months after injection ceased (Ellsworth, 2013, Keranen et al., 2014). Notably, this phenomenon has been documented in the context of wastewater disposal activities and may not be directly applicable to hydraulic fracturing operations, which differ in injection volumes, pressures, and durations.

One of the critical components of seismic hazard assessments is to quantify the propensity of a specific site to generate seismicity in response to fluid injection (Schultz et al., 2017). This study systematically investigates the spatiotemporal occurrence of induced seismicity associated with HF activities within the South Montney Play. We employ the seismogenic index to provide robust statistical measures of the likelihood of induced seismicity based on the volume of injected fluid, thereby to better understand the resulting seismicity pattern (Shapiro et al., 2010, Dinske and Shapiro, 2013). The application of the seismogenic index involves detailed analysis of the spatiotemporal clustering of seismicity and the extraction of seismological parameters for individual clusters (McClure et al., 2017, Dokht et al., 2021). This approach allows for the identification of areas with higher seismic potential and the assessment of how different parameters, such as injection volume, influence seismic activity. By using statistical models based on the seismogenic index, this study aims to enhance the accuracy and reliability of seismic hazard assessments, offering a data-driven framework for predicting the maximum expected magnitudes of induced seismic events. This not only aids in risk management and mitigation strategies but also contributes to the broader understanding of induced seismicity in complex geological settings.

Datasets and Methods

Earthquake Catalogs and Injection Datasets

The dataset used in this study comprises earthquake catalogs compiled by NRCan's Induced Seismicity Research (ISR) Project and the Canadian National Earthquake Database between January 2017 and September 2023 (Visser et al., 2017, 2021). After removing duplicate events, the final dataset consists of 41,586 events, of which 38,706 occurred within the South Montney Play. Earthquake magnitudes range between -1.8 and 4.2, with an average depth of 1.9 km (Figure 1a). The earthquake catalog provides an average location uncertainty of approximately 1.5 km, estimated at the 68% confidence level. However, it is important to note that the statistically measured depth error may somewhat underestimate the actual depth uncertainty, possibly due to limitations in the observational data or the underlying assumptions in the earthquake location process. This comprehensive dataset provides a robust foundation for detailed analysis and understanding of the spatial and temporal patterns of induced seismicity associated with HF operations in the South Montney Play of northeastern British Columbia, Canada.

According to the BC Energy Regulator (BCER), there were 1,450 active HF wells in the study area during the specified period (see Figure 1b). To analyze the spatiotemporal occurrence of injection-induced earthquakes (IIEs) at different injection sites, we utilized the Density-Based Spatial Clustering of Applications with Noise (DBSCAN) algorithm. This method grouped HF wells based on their (1) target formations, (2) surface locations, and (3) operational timelines. The DBSCAN clustering process identified a total of 535 clusters of HF injection wells. Each cluster of HF wells represents a group of horizontal wells that are spatially and temporally related, with a focus on a specific target formation. Notably,

our clustering approach distinguishes between HF injection clusters targeting different formations, ensuring that each cluster is associated with a single formation. This method effectively separates wells targeting the Upper Montney (UM), Upper-Middle Montney (UMM), Lower-Middle Montney (LMM), or Lower Montney (LM) formations. The majority of these clusters of HF wells (51%) target the Upper Montney (UM) formation, followed by approximately 33% targeting the Lower-Middle Montney (LMM) formation (Table 1). It should be emphasized that these clusters are defined based on injection activity and do not inherently correspond to seismogenic clusters associated with induced seismicity (the association between injection and seismicity, as well as the identification of seismogenic clusters, will be discussed later in this section). This refined clustering approach facilitates a more detailed analysis of seismicity patterns, accounting for potential variations based on the specific target formation. It is important to note that each well pad may host multiple horizontal wells, and our clustering method accounts for this by grouping wells that are co-located and contemporaneously active, while still distinguishing between different target formations. This ensures that the analysis accurately reflects the operational practices and geological targets within the study area.

Table 1: Number of individual HF wells (second column) and Number of HF clusters (third column) based on the corresponding target formation (UM: Upper Montney; UMM: Upper-Middle Montney; LMM: Lower-Middle Montney; LM: Lower Montney).

Target formation	Number of HF wells	Number of HF clusters
UM	969	273
UMM	128	80
LMM	347	177
LM	6	5

We follow the approach proposed by Schultz et al. (2018) and Wang et al. (2024) to establish the spatiotemporal correlation between IIEs and HF operations. To attribute each IIE to its corresponding HF well, the induced event should occur within a time window bounded by the completion of the first fracking stage and 7 days after the completion of the final stage. In addition, we consider a maximum distance of 5 km between the IIE and the HF well as the spatial threshold. This distance accounts for potential uncertainties in earthquake locations reported in the original earthquake catalogs (Figure 2). An induced event is associated with a specific injection site if it satisfies both the temporal and spatial criteria outlined above. In cases where multiple injection clusters meet these spatiotemporal criteria, the seismicity is

assigned to the injection cluster targeting the LMM member. If none of the eligible injection clusters targets the LMM, the event is attributed to the closest injection site.

By applying the aforementioned IIE-HF well association criteria, we identified 70 clusters of induced seismicity within the LMM formation, followed by 10 clusters within the UM formation. While there are only 3 clusters of induced seismicity within the Upper-Middle Montney (UMM) formation, none of the recorded seismic events were associated with HF injection wells targeting the Lower Montney (LM) formation. It is worth mentioning that to ensure reliable estimates for the seismicity characterization parameters, we considered only those clusters of induced seismicity that have more than 50 IIEs associated with them. These findings suggest that approximately 84% of these induced seismicity clusters were associated with HF operations targeting the LMM formation, despite the fact that the largest cumulative fluid volume ($\sim$1.54$\times$10^{7}m^3) was injected into the UM formation during the study period. The LMM formation received a comparatively lower injected volume of $\sim$5.98$\times$10^{6}m^3 (Figure 3). From the seismicity perspective, 36,170 events are associated with HF wells within the South Montney Play; 2,859 of the associated events have magnitudes of 1.5 or greater, and 558 have magnitudes of 2 or greater. Of these, 33,322 events are linked to HF wells targeting the LMM formation (nearly 92% of the total IIEs), while only 2,026 and 822 events are attributed to injection activities within the UM and UMM formations, respectively (Figure 4 shows three examples of IIE-HF well associations for different target formations).

Seismogenic Index

To assess the potential for induced seismicity associated with fluid injection operations, such as hydraulic fracturing, we adopt a site-specific quantitative parameter known as the seismogenic index, introduced by Shapiro et al. (2010). The seismogenic index provides a means to compare the relative seismic activity in different regions under different operational conditions, and help us quantify the likelihood of seismic event occurrence in response to fluid injection. To obtain an estimate of the seismogenic index, Σ, we consider the cumulative injected volume after time t, $Qc(t)$, and the total number of associated events with magnitudes above a predetermined magnitude threshold M, $N_M(t)$, within each cluster of induced seismicity (Shapiro et al., 2010, Dinske and Shapiro, 2013):

$$\Sigma = logN_M(t) - logQc(t) + bM, \tag{1}$$

In this equation, the b-value is the slope of the Gutenberg-Richter relation obtained for each induced seismicity cluster, independently, and we use the magnitude of completeness of the entire catalog as the magnitude threshold (see Figure 1a). It should be emphasized that to ensure reliable estimates of the seismogenic indices, we selected clusters of induced seismicity with more than 50 IIEs. The seismogenic index was then calculated by integrating these components, allowing us to assess the propensity of different clusters to generate seismic events. A higher seismogenic index indicates a greater likelihood of seismicity for a given volume of fluid injection. This analysis provides insight into the spatial variability of seismicity within the South Montney Play and aids in identifying areas with a higher risk of induced seismicity. In the next section, we investigate the effect of injection activity on induced seismicity and introduce seismogenic index models tailored for each specific injection site.

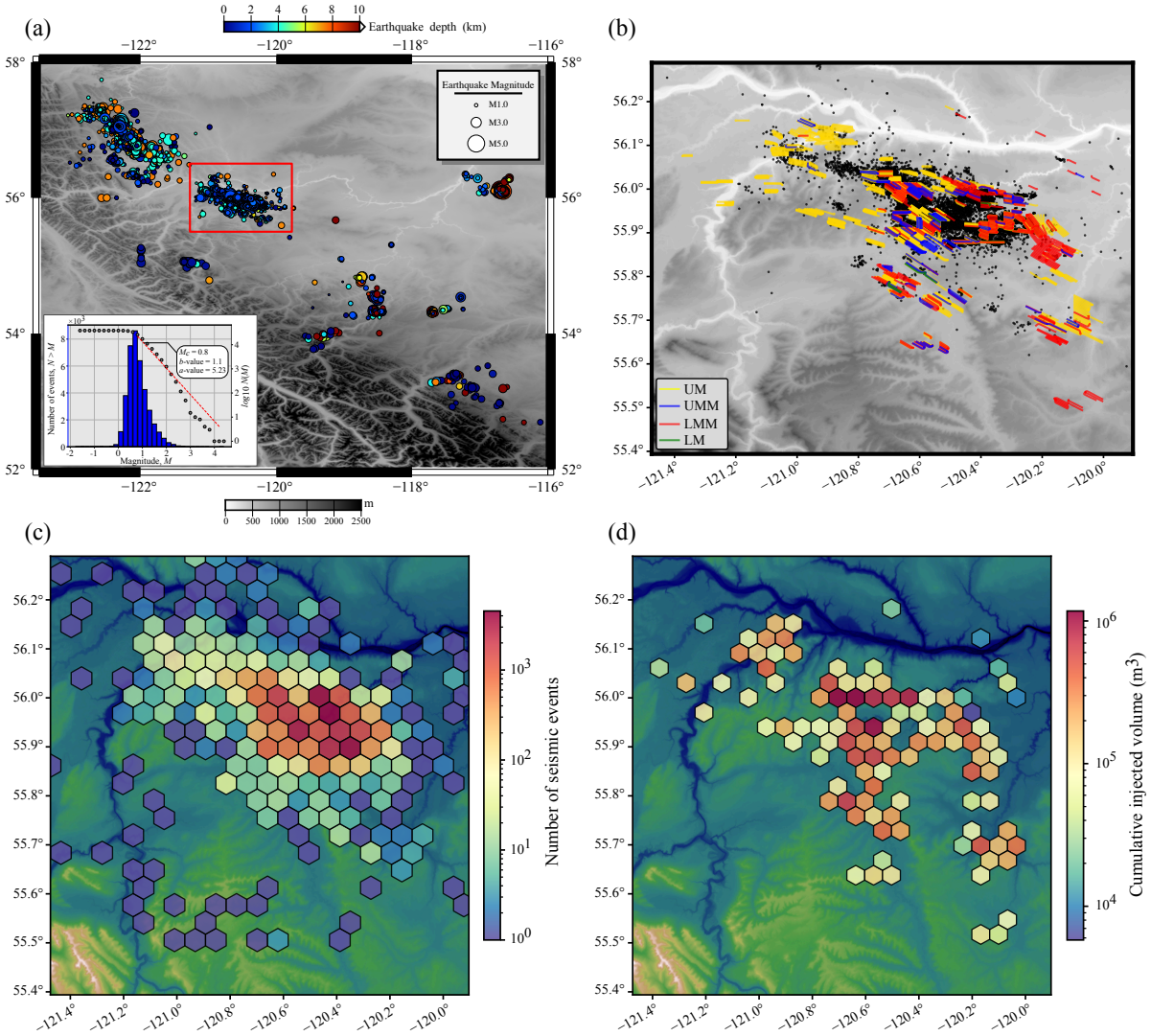

Figure 1: (a) Spatial distribution of seismicity in northeastern British Columbia and western Alberta. Cold and warm colors represent shallow and deep earthquakes. The inset figure shows the frequency-magnitude (FM) distribution and the corresponding Gutenberg-Richter (GR) relation parameters for seismicity within the South Montney Play (outlined by the red rectangle) from January 2017 to August 2023. (b) Distribution of hydraulic fracturing (HF) wells operating during the study period. Different colors represent the target formation for each individual well; UM: Upper Montney, UMM: Upper-Middle Motney, LMM: Lower-Middle Motney, and LM: Lower Montney. Black dots represent the background seismicity. (c) and (d) Hexagonal binned plots showing the earthquake counts and cumulative HF volume, respectively, for the entire study period.

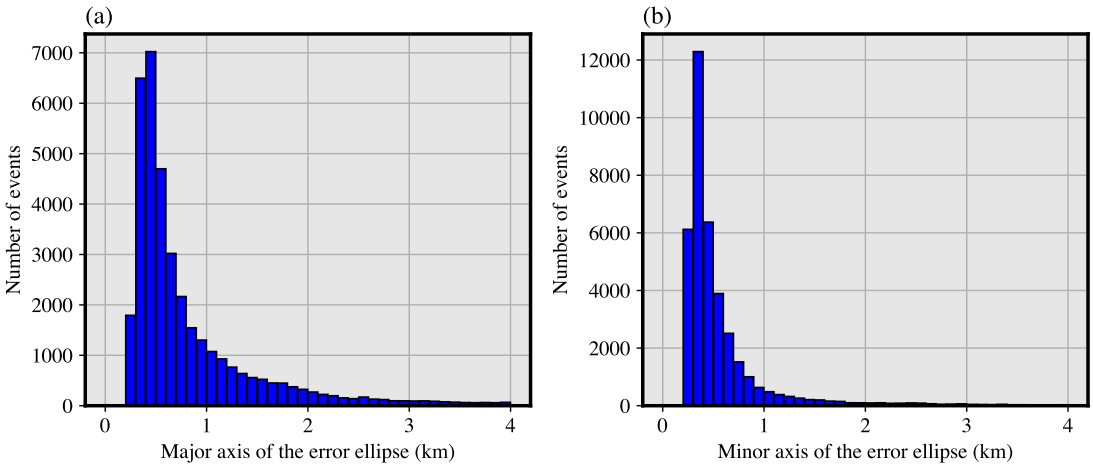

Figure 2: Distributions of the lengths of the (a) major and (b) minor axes of the horizontal error ellipses obtained from the enhanced GSC catalogs. The average lengths for the major and minor axes are 0.9 ($\pm$0.6) and 0.6 km ($\pm$0.5), respectively.

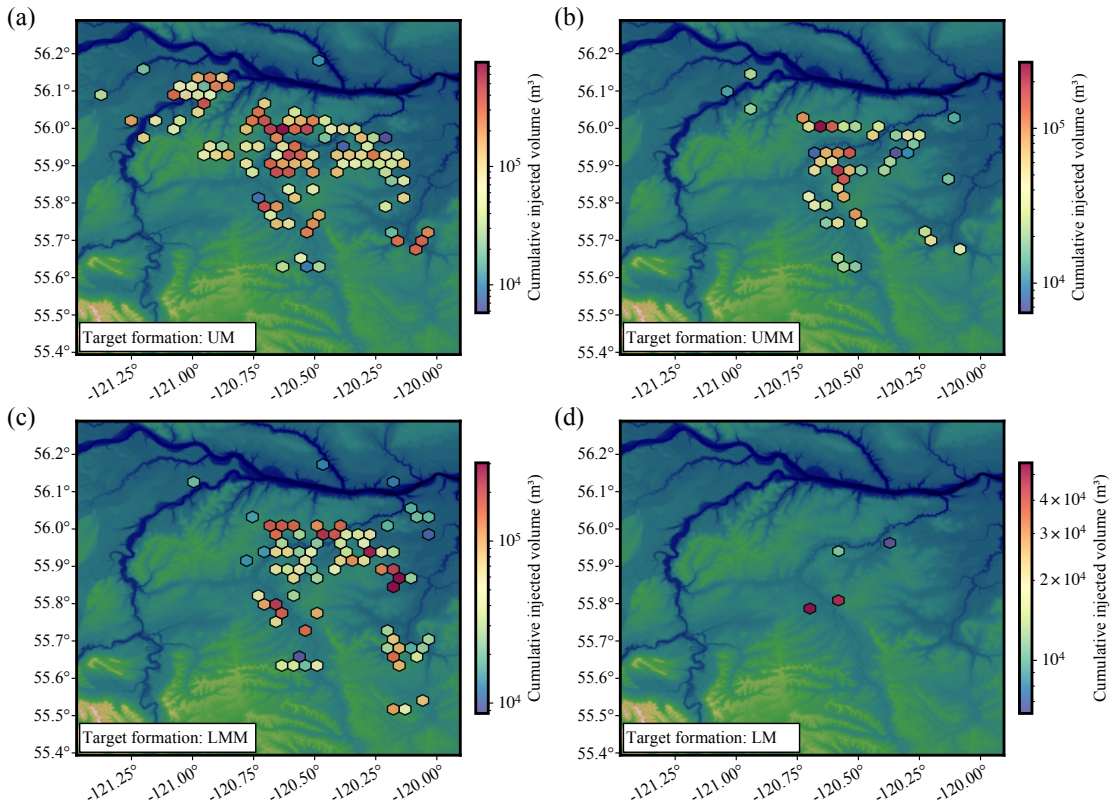

Figure 3: Hexagonal binned plots showing the spatial distributions of the cumulative injected volume due to the HF operations associated with the (a) Upper Montney (UM), (b) Upper-Middle Montney (UMM), (c) Lower-Middle Montney (LMM) and (d) Lower Montney (LM) formations. We observe the respective cumulative injected volumes of approximately 1.54×10^7, 2.55×10^6, 5.98×10^6 and $1.22\times10^6 m^3$ for the UM, UMM, LMM and LM formations.

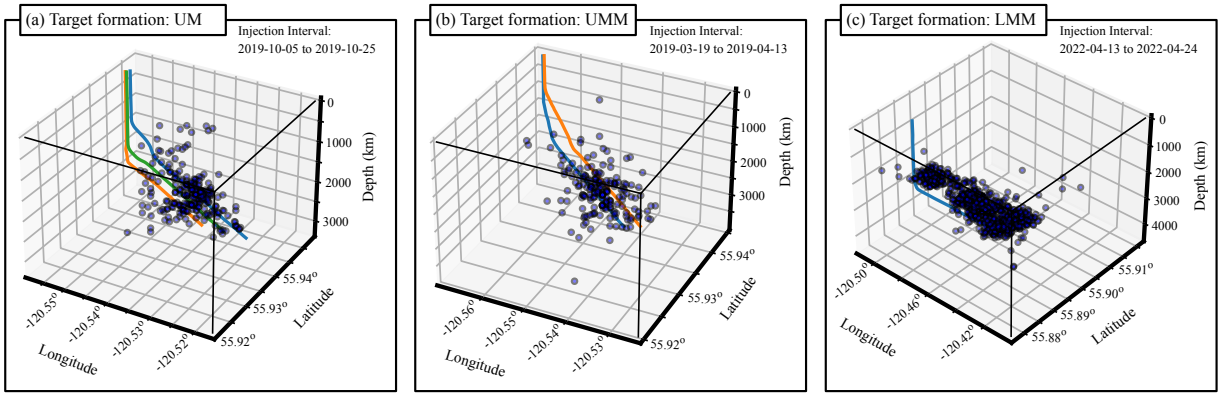

Figure 4: Three examples of IIE-HF well associations for the HF wells targeting the (a) Upper Montney, (b) Upper-Middle Montney and (c) Lower-Middle Montney formations. Blue circles represent seismic events.

Results

The first step in our analysis involved determining the b-value from the Gutenberg-Richter (GR) frequency-magnitude (FM) relation for individual clusters of induced seismicity. The b-value is a crucial parameter that provides insights into the relative proportion of large to small earthquakes in a given region or sequence. Several studies have investigated the factors influencing the b-value and its variations, suggesting that it is related to the stress regime and the heterogeneity of the medium (Bachmann et al., 2012, Reyes et al., 2013, Kamer and Hiemer, 2015, Martínez-Álvarez et al., 2015, Singh and Singh, 2015). While a b-value of around 1.0 is often considered typical for tectonic earthquakes (Frohlich and Davis, 1993, Hiemer et al., 2014), significant deviations from this value have been observed for localized seismicity associated with anthropogenic activities such as fluid injection, with b-values ranging from 0.5 to greater than 2.5 (Dinske and Shapiro, 2013, Eaton et al., 2014, Van der Elst et al., 2016, Mousavi et al., 2017, Khajehdehi et al., 2022).

We calculated the b-value for each individual cluster of IIEs using the Aki-Utsu maximum likelihood method (Aki, 1965), which has been widely used to obtain the GR relation parameters in induced seismicity (Verdon and Budge, 2018, Kwiatek et al., 2019, Babaie Mahani, 2021). This approach ensures a statistically robust estimation of the b-value for our seismic data analysis. Lower b-values indicate a relative increase in the occurrence of larger earthquakes, while higher b-values indicate a predominance of smaller earthquakes. We obtained estimates of b-values for 83 IIE clusters within the South Montney Play, ranging between 0.51 and 2.3 (Figure 5a). The minimum b-value was observed in the western part of the study area, in the cluster with the largest IIE, which had a local magnitude (M_L) of 4.2. The spatial variations in b-values do not show a clear lateral pattern and appear to be more randomly distributed. However, as expected, its spatial distribution shows a weak negative correlation

with the magnitude of the largest event in each cluster of IIEs (see Figures 5a and 9a).

Using the estimated b-values for the clusters of induced seismicity and a constant magnitude cut-off of 0.8, we derived the seismogenic indices, Σ, to assess the induced seismicity hazard potential at each injection site. A spatially invariant cut-off magnitude, equal to the magnitude of completeness of the entire catalog, was applied to ensure consistent measurements across all clusters of IIEs. This approach guarantees that our analysis considers only those seismic events that are reliably detected and recorded, thereby enhancing the robustness of our results. The Σ values at the end of injection activity at IIE clusters range from -2.9 to 0.3 (see Figure 5b). Notably, the highest seismogenic indices are associated with the southern clusters, which exhibit an average Σ value of greater than -0.5, suggesting a higher induced seismicity hazard potential in these regions. The observed spatial correlation between the estimated seismogenic indices and the number of significant seismic events aligns with the fundamental concept of the seismogenic index, which posits that higher Σ values correspond to regions with greater seismic activity due to injection operations (see Figures 5b and 6). This correlation further validates the use of seismogenic indices as a reliable measure to estimate the occurrence probabilities of seismic events induced by fluid injection.

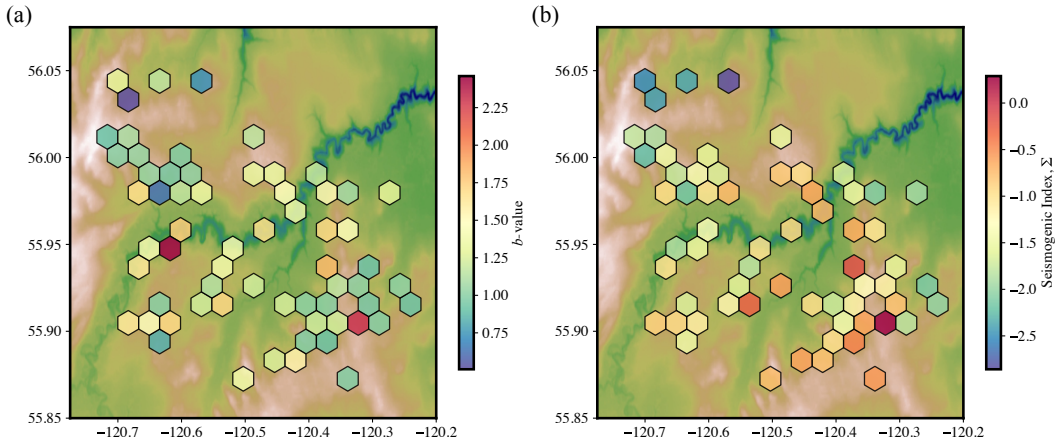

Figure 5: Spatial distributions of the average estimates of the (a) b-values and (b) seismogenic indices in the study area.

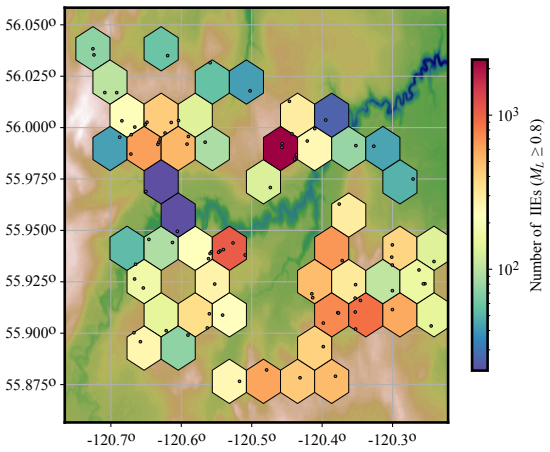

Figure 6: Spatial distribution of the number of IIEs of significant magnitudes within the South Montney Play. The small circles indicate the measuring points (i.e., seismicity clusters).

Discussion

The seismogenic index provides a quantitative measure to assess the potential for induced seismicity associated with fluid injection operations. By integrating parameters such as the cumulative injected volume, the number of induced events above a magnitude threshold, and the b-value of the Gutenberg-Richter relation, the seismogenic index allows for characterizing the seismicity hazard at a given injection site. In this study, we first calculated site-specific b-values for individual clusters of induced seismicity. The overall range and average estimate of the b-value are consistent with typical values reported in previous studies investigating induced seismicity, particularly in western Canada (Eaton et al., 2014, Verdon and Budge, 2018, Babaie Mahani, 2021, Salvage et al., 2021, Salvage and Eaton, 2022). It is important to note that while the average b-value provides a general characterization of the seismicity, spatial variations in b-values were observed across the study area (see Figure 5a). These variations may be attributed to local differences in factors such as stress conditions, pore pressure perturbations, and geological heterogeneities, which can influence the relative proportions of large and small events (Bachmann et al., 2012, Reyes et al., 2013).

Building upon the calculated b-values, we derived the seismogenic indices for the clusters of IIEs within the South Montney Play. The resulting seismogenic indices not only help distinguish relative seismic hazards between different clusters but also enable us to calculate magnitude exceedance probability functions for each HF site. These probability functions are critical for understanding the likelihood of seismic events exceeding specific magnitudes given an injection scenario. It is important to acknowledge that the potential for seismicity can be affected by traffic light systems and mitigation strategies implemented by operators when induced events of significant magnitudes are detected. This implies that the likelihood of larger events may be reduced by halting fracking to allow pressure to dissipate gradually, or by

adjusting the rate and pressure of injection. Operators' mitigation methods include varying wait times, altering stage lengths, modifying perforation clustering, changing fluid viscosity, or skipping stages. The choice of mitigation depends on observed seismicity patterns, geological conditions, and well construction. Although challenging to measure or quantify, the dynamic nature of injection operations can significantly influence the seismogenic potential (Bommer et al., 2015, Maxwell et al., 2015).

Assuming a non-homogeneous Poisson process for induced events, Shapiro et al. (2010) demonstrated that the probability that an event exceeding magnitude M does not occur when a total volume of $Qc(t)$ is injected, in the time interval from 0 until t, can be calculated as:

$$\mathbb{P}(0, M, Qc(t)) = exp(-Qc(t) \times 10^{\Sigma - bM}). \tag{2}$$

Therefore, the occurrence probabilities of induced events with magnitude larger than M can be obtained as 1 - $\mathbb{P}(0, M, Qc(t))$ (Shapiro et al., 2010, Langenbruch and Zoback, 2016). The resulting magnitude exceedance probabilities illustrate distinct seismic responses to injection operation, given site-specific seismogenic parameters. In other words, exceedance probabilities cannot be generalized across different sites without adjusting the seismogenic index based on site-specific observations.

Figure 7 presents the normalized exceedance probability functions for three distinct HF injection scenarios targeting different formations within the South Montney Play. The results reveal key differences in the probabilities of generating larger magnitude events and their relationships with injected volume, seismogenic index, and b-value of the GR relation. The IIEs associated with these wells exhibit the largest magnitudes of 2.0, 2.0 and 4.2, respectively (marked by red dashed lines in Figures 7a-c). The UM and UMM wells, with respective injected volumes of $\sim 8.6 \times 10^4\ m^3$ and $\sim 1.15 \times 10^5\ m^3$, demonstrate probabilities of nearly 86% (the former) and 97% (the latter) for inducing events with $M \geq 2.0$ (Figures 7a and 7b). The LMM case, despite a significantly low injection volume of about $80 \times 10^2\ m^3$, exhibits a probability of 25% for exceeding a magnitude of 4.2 or larger (Figure 7c). Notably, for the UM and UMM wells, the probability of inducing larger events drops sharply and approaches zeros for $M \geq 4$ despite larger injection volumes compared to the LMM case. The results indicate that injected volume alone does not control the probability of generating large

seismic events. While the presented UM and UMM sites received significantly larger injection volumes than the LMM site, the probability of inducing large events at these locations remains negligible. This discrepancy suggests that other factors, such as geological properties of the target formations (e.g., fault density and stress regime) and operational conditions, play a critical role in influencing the likelihood of triggering larger seismic events.

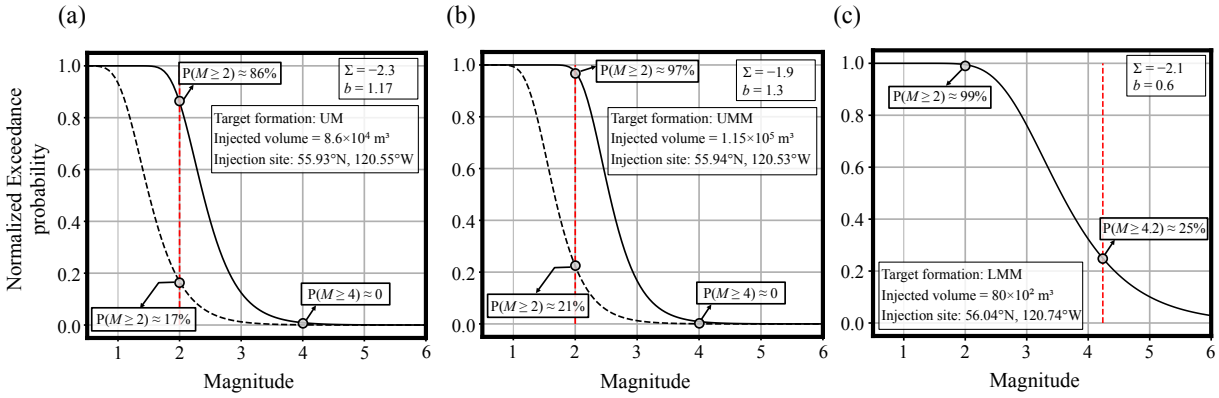

Figure 7: Magnitude exceedance probability functions for three HF injection scenarios targeting the (a) Upper Montney, (b) Upper-Middle Montney, and (c) Lower-Middle Montney formations. The exceedance probability functions are obtained based on the reported injected volumes and the estimates of Σ and b-values at the corresponding HF injection sites. Red dashed lines indicate the magnitudes of the largest IIEs recorded during injection. Black dashed curves in panels a and b show the probability functions obtained using an injection volume of $80{\times}10^2\ m^3$.

To provide a mitigation strategy, Verdon and Budge (2018) utilize the seismogenic index framework to forecast the maximum magnitude of IIEs that will not be exceeded at a given confidence level, χ. By rearranging Equation 2, we obtain:

$$M_{Max}^{\Sigma\chi} = \frac{\Sigma - \log(\frac{-\ln(\chi)}{Qc})}{b}. \tag{3}$$

This is an entirely statistical, data-driven approach that is based on the seismicity observations and injection parameters. For each seismogenic HF well, we calculate the maximum magnitude forecasts of IIEs that will not be exceeded by the end of injection interval at the 68% confidence interval. A general positive correlation between the observed and forecasted M_L values of the largest IIEs is evident (Figure 8), with their corresponding spatial patterns showing an overall agreement (Figure 9). These observations indicate that the statistical model can provide a reasonably upper bound (i.e., the magnitude envelope) for the maximum size of induced events. It is worth emphasizing that this approach is based on the principal

assumption that the seismogenic index and GR b-value will remain constant throughout the injection activity. However, various factors, such as $in\ situ$ stress conditions and the presence of pre-existing fracture networks, can influence these parameters. Growing pore-pressure front due to hydraulic fracturing operation and its interaction with the pre-existing fault zone or layers that are more prone to seismic activity may significantly influence the seismic response and result in abrupt changes in the seismological parameters (Langenbruch and Zoback, 2016, Schultz et al., 2018, Verdon and Budge, 2018, Tan et al., 2020). Given these concerns, to provide an appropriate mitigation strategy requires a detailed examination of these seismic parameters during HF stimulation.

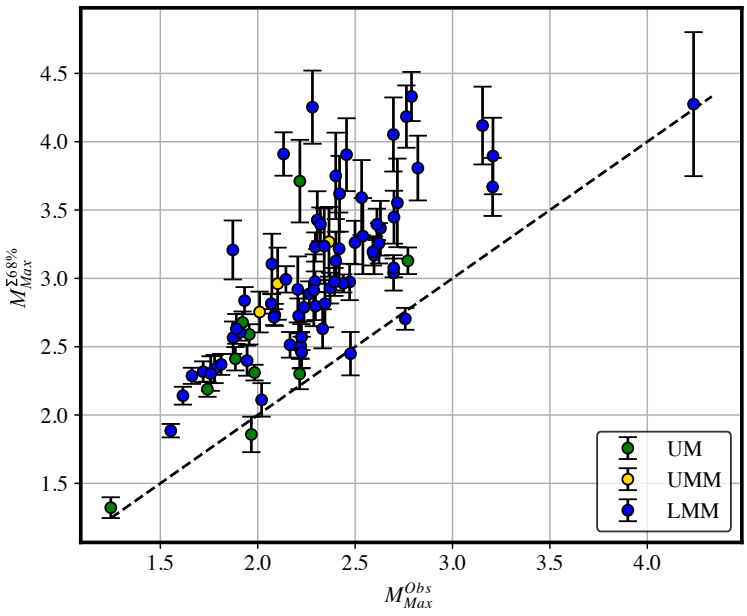

Figure 8: Comparison between the largest observed magnitudes, M_{Max}^{Obs}, and forecasts of the largest induced events obtained using the seismogenic index at 68% confidence level, $M_{Max}^{\Sigma 68}$, for individual HF wells.

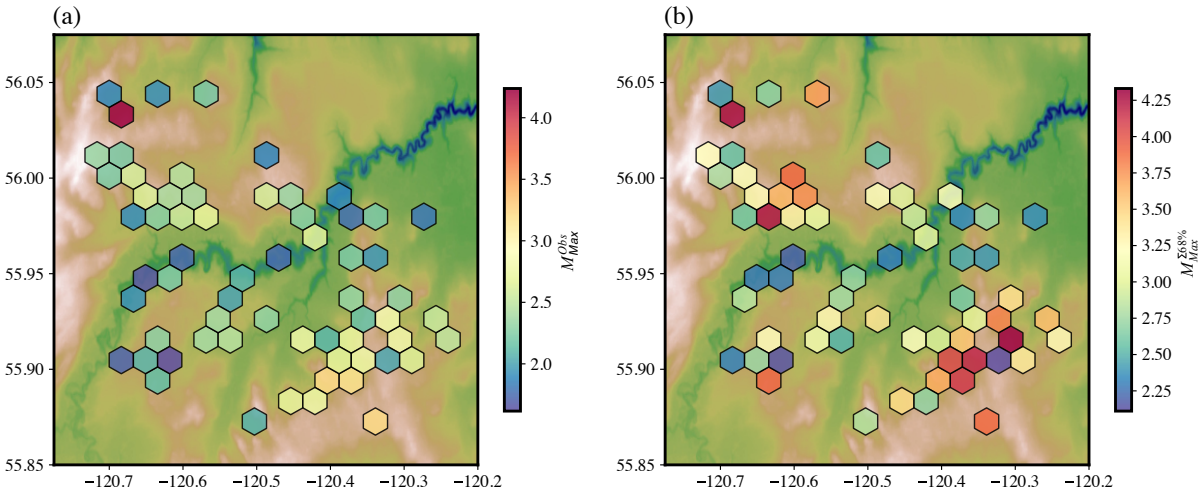

Figure 9: Spatial distributions of the (a) largest observed magnitudes, M_{Max}^{Obs}, and (b) forecasts of the largest induced events obtained using the seismogenic index at 68% confidence level, $M_{Max}^{\Sigma 68}$.

Conclusions

This study provides a comprehensive analysis of induced seismicity associated with hydraulic fracturing operations in the South Montney Play. Our findings highlight the spatial variability of seismic response to injection activities across different formations. The Lower-Middle Montney formation shows a higher propensity for induced seismicity despite receiving less injected fluid volume compared to the Upper Montney formation. This suggests that factors beyond injection volume, such as local geological conditions and stress states, play crucial roles in determining seismic response.

The calculated b-values and seismogenic indices offer valuable insights into the characteristics of induced seismicity at different injection sites. The wide range of b-values (0.51 to 2.3) indicates significant variations in the relative proportions of large to small earthquakes across the study area. Similarly, the range of seismogenic indices (-2.9 to 0.3) reflects the varying potential for induced seismicity at different locations within the play.

Robust estimation of site-specific parameters, such as the seismogenic index and b-value, enables reliable measurement of magnitude exceedance probabilities, which are crucial for risk assessment and mitigation strategies. By providing a quantitative framework to evaluate the likelihood of induced seismic events, this study contributes to the development of more informed and targeted approaches to managing induced seismicity risks associated with hydraulic fracturing operations. Future work should focus on integrating additional geological and operational data to further refine our understanding of the factors controlling induced seismicity in this region.

Acknowledgements

We would like to acknowledge the BC Oil and Gas Research and Innovation Society (BC OGRIS) for funding this research project. We also appreciate the discussions, input, support, and feedback provided during the project by Stuart Venables and Michelle Gaucher of the BC Energy Regulator (BCER).

References

Aki, K. (1965), 'Maximum likelihood estimate of b in the formula log N= a-bM and its confidence limits', *Bull. Earthquake Res. Inst., Tokyo Univ.* **43**, 237–239.

Atkinson, G. M., Eaton, D. W., Ghofrani, H., Walker, D., Cheadle, B., Schultz, R., Shcherbakov, R., Tiampo, K., Gu, J., Harrington, R. M. et al. (2016), 'Hydraulic fracturing and seismicity in the Western Canada Sedimentary Basin', *Seismological research letters* **87**(3), 631–647.

Atkinson, G. M., Eaton, D. W. and Igonin, N. (2020), 'Developments in understanding seismicity triggered by hydraulic fracturing', *Nature Reviews Earth & Environment* **1**(5), 264–277.

Babaie Mahani, A. (2021), 'Seismic b value within the Montney play of northeastern British Columbia, Canada', *Canadian Journal of Earth Sciences* **58**(8), 720–730.

Babaie Mahani, Alireza, A. B., Kao, H., Atkinson, G. M., Assatourians, K., Addo, K. and Liu, Y. (2019), 'Ground-motion characteristics of the 30 November 2018 injection-induced earthquake sequence in northeast British Columbia, Canada', *Seismological Research Letters* **90**(4), 1457–1467.

Bachmann, C. E., Wiemer, S., Goertz-Allmann, B. and Woessner, J. (2012), 'Influence of pore-pressure on the event-size distribution of induced earthquakes', *Geophysical Research Letters* **39**(9).

Bommer, J. J., Crowley, H. and Pinho, R. (2015), 'A risk-mitigation approach to the management of induced seismicity', *Journal of Seismology* **19**, 623–646.

Dinske, C. and Shapiro, S. A. (2013), 'Seismotectonic state of reservoirs inferred from magnitude distributions of fluid-induced seismicity', *Journal of seismology* **17**, 13–25.

Dokht, R. M., Kao, H., Babaie Mahani, A. and Visser, R. (2021), 'Spatiotemporal analysis of seismotectonic state of injection-induced seismicity clusters in the western Canada sedimentary basin', *Journal of Geophysical Research: Solid Earth* **126**(4), e2020JB021362.

Eaton, D. W., Davidsen, J., Pedersen, P. K. and Boroumand, N. (2014), 'Breakdown of the Gutenberg-Richter relation for microearthquakes induced by hydraulic fracturing: Influence of stratabound fractures', *Geophysical Prospecting* **62**(4-Vertical Seismic Profiling and Microseismicity Frontiers), 806–818.

Ellsworth, W. L. (2013), 'Injection-induced earthquakes', *science* **341**(6142), 1225942.

Frohlich, C. and Davis, S. D. (1993), 'Teleseismic b values; or, much ado about 1.0', *Journal of Geophysical Research: Solid Earth* **98**(B1), 631–644.

Hiemer, S., Woessner, J., Basili, R., Danciu, L., Giardini, D. and Wiemer, S. (2014), 'A smoothed stochastic earthquake rate model considering seismicity and fault moment release for Europe', *Geophysical Journal International* **198**(2), 1159–1172.

Hui, G., Chen, S., Gu, F., Pang, Y., Yu, X. and Zhang, L. (2021), 'Insights on controlling factors of hydraulically induced seismicity in the Duvernay East Shale Basin', *Geochemistry, Geophysics, Geosystems* **22**(2), e2020GC009563.

Jia, S. Q., Wong, R. C. and Eaton, D. W. (2022), 'Characterization of damage processes in Montney siltstone under triaxial compression using acoustic emission and diagnostic imaging', *Geophysical Journal International* **228**(3), 2005–2017.

Kamer, Y. and Hiemer, S. (2015), 'Data-driven spatial b value estimation with applications to California seismicity: To b or not to b', *Journal of Geophysical Research: Solid Earth* **120**(7), 5191–5214.

Keranen, K. M., Weingarten, M., Abers, G. A., Bekins, B. A. and Ge, S. (2014), 'Sharp increase in central Oklahoma seismicity since 2008 induced by massive wastewater injection', *Science* **345**(6195), 448–451.

Khajehdehi, O., Eaton, D. W. and Davidsen, J. (2022), 'Spatiotemporal clustering of seismicity in the Kiskatinaw seismic monitoring and mitigation area', *Frontiers in Earth Science* **10**, 894549.

Kwiatek, G., Saarno, T., Ader, T., Bluemle, F., Bohnhoff, M., Chendorain, M., Dresen, G., Heikkinen, P., Kukkonen, I., Leary, P. et al. (2019), 'Controlling fluid-induced seismicity during a 6.1-km-deep geothermal stimulation in Finland', *Science Advances* **5**(5), eaav7224.

Langenbruch, C. and Zoback, M. D. (2016), 'How will induced seismicity in Oklahoma respond to decreased saltwater injection rates?', *Science advances* **2**(11), e1601542.

Martínez-Álvarez, F., Gutiérrez-Avilés, D., Morales-Esteban, A., Reyes, J., Amaro-Mellado, J. L. and Rubio-Escudero, C. (2015), 'A novel method for seismogenic zoning based on triclustering: application to the Iberian Peninsula', *Entropy* **17**(7), 5000–5021.

Maxwell, S., Zhang, F. and Damjanac, B. (2015), 'Geomechanical modeling of induced seismicity resulting from hydraulic fracturing', *The Leading Edge* **34**(6), 678–683.

McClure, M., Gibson, R., Chiu, K.-K. and Ranganath, R. (2017), 'Identifying potentially induced seismicity and assessing statistical significance in Oklahoma and California', *Journal of Geophysical Research: Solid Earth* **122**(3), 2153–2172.

Mousavi, S. M., Ogwari, P. O., Horton, S. P. and Langston, C. A. (2017), 'Spatio-temporal evolution of frequency-magnitude distribution and seismogenic index during initiation of induced seismicity at Guy-Greenbrier, Arkansas', *Physics of the Earth and Planetary Interiors* **267**, 53–66.

Peña Castro, A., Roth, M., Verdecchia, A., Onwuemeka, J., Liu, Y., Harrington, R., Zhang, Y. and Kao, H. (2020), 'Stress chatter via fluid flow and fault slip in a hydraulic fracturing-induced earthquake sequence in the Montney Formation, British Columbia', *Geophysical Research Letters* **47**(14), e2020GL087254.

Reyes, J., Morales-Esteban, A. and Martínez-Álvarez, F. (2013), 'Neural networks to predict earthquakes in Chile', *Applied Soft Computing* **13**(2), 1314–1328.

Riazi, N., Eaton, D. W., Aklilu, A. and Poulin, A. (2020), 'Application of focal-time analysis for improved induced seismicity depth control: A case study from the Montney Formation, British Columbia, Canada', *Geophysics* **85**(6), KS185–KS196.

Salvage, R., Dettmer, J., Swinscoe, T., MacDougall, K., Eaton, D., Stacey, M., Aboud, M., Kang, T., Kim, S. and Rhie, J. (2021), 'Real-time monitoring of seismic activity in

the Kiskatinaw area, northeastern British Columbia', *Geoscience BC Summary of Activities 2020: Energy and Water, Geoscience BC, Report 2021* **2**, 17–30.

Salvage, R. O. and Eaton, D. W. (2022), 'The influence of a transitional stress regime on the source characteristics of induced seismicity and fault activation: Evidence from the 30 November 2018 Fort St. John ML 4.5 induced earthquake sequence', *Bulletin of the Seismological Society of America* **112**(3), 1336–1355.

Schultz, R., Atkinson, G., Eaton, D. W., Gu, Y. J. and Kao, H. (2018), 'Hydraulic fracturing volume is associated with induced earthquake productivity in the Duvernay play', *Science* **359**(6373), 304–308.

Schultz, R., Wang, R., Gu, Y. J., Haug, K. and Atkinson, G. (2017), 'A seismological overview of the induced earthquakes in the Duvernay play near Fox Creek, Alberta', *Journal of Geophysical Research: Solid Earth* **122**(1), 492–505.

Shapiro, S. A., Dinske, C., Langenbruch, C. and Wenzel, F. (2010), 'Seismogenic index and magnitude probability of earthquakes induced during reservoir fluid stimulations', *The Leading Edge* **29**(3), 304–309.

Singh, C. and Singh, S. (2015), 'Imaging b-value variation beneath the Pamir–Hindu Kush region', *Bulletin of the Seismological Society of America* **105**(2A), 808–815.

Tan, Y., Hu, J., Zhang, H., Chen, Y., Qian, J., Wang, Q., Zha, H., Tang, P. and Nie, Z. (2020), 'Hydraulic fracturing induced seismicity in the southern Sichuan Basin due to fluid diffusion inferred from seismic and injection data analysis', *Geophysical Research Letters* **47**(4), e2019GL084885.

Van der Elst, N. J., Page, M. T., Weiser, D. A., Goebel, T. H. and Hosseini, S. M. (2016), 'Induced earthquake magnitudes are as large as (statistically) expected', *Journal of Geophysical Research: Solid Earth* **121**(6), 4575–4590.

Verdecchia, A., Wang, B., Liu, Y., Harrington, R., Roth, M., Castro, A. P. and Onwuemeka, J. (2020), Exploring possible causative mechanisms for earthquakes triggered by hydraulic fracturing: examples from the Montney Basin, BC, Canada., number EGU2020-10680, Copernicus Meetings.

Verdon, J. P. and Budge, J. (2018), 'Examining the capability of statistical models to mitigate induced seismicity during hydraulic fracturing of shale gas reservoirs', *Bulletin of the Seismological Society of America* **108**(2), 690–701.

Visser, R., Kao, H., Dokht, R., Mahani, A. and Venables, S. (2021), *A comprehensive earthquake catalogue for northeastern British Columbia: The northern Montney trend from 2017 to 2020 and the Kiskatinaw Seismic Monitoring and Mitigation Area from 2019 to 2020*, Geological Survey of Canada.

Visser, R., Smith, B., Kao, H., Babaie Mahani, A., Hutchinson, J. and McKay, J. (2017), *A comprehensive earthquake catalogue for northeastern British Columbia and western Alberta, 2014-2016*, Geological Survey of Canada.

Wang, B., Kao, H., Dokht, R. M., Visser, R. and Yu, H. (2022), 'Delineating the controlling factors of hydraulic fracturing-induced seismicity in the northern Montney Play, northeastern British Columbia, Canada, with machine learning', *Seismological Society of America* **93**(5), 2439–2450.

Wang, B., Kao, H., Yu, H., Li, G., Dokht, R. M. and Visser, R. (2024), 'Unveiling Key factors governing seismogenic potential and seismogenic productivity of hydraulic fracturing pads: Insights from machine learning in the Southern Montney Play', *Earth and Planetary Science Letters* **626**, 118511.

Wozniakowska, P. and Eaton, D. W. (2020), 'Machine learning-based analysis of geological susceptibility to induced seismicity in the Montney Formation, Canada', *Geophysical Research Letters* **47**(22), e2020GL089651.

Yu, H., Harrington, R. M., Liu, Y. and Wang, B. (2019), 'Induced seismicity driven by fluid diffusion revealed by a near-field hydraulic stimulation monitoring array in the Montney Basin, British Columbia', *Journal of Geophysical Research: Solid Earth* **124**(5), 4694–4709.